Title: Modeling the single particle crushing behavior by random discrete element method

Authors: Du-min Kuang[a], Zhi-lin Long[a], Tao Zhao[c], Biao Luo[a,b], Ikechukwu Ogwu[d], Feng-lan Kuang[a]

Affiliations:

a. College of Civil Engineering, Xiangtan University, Xiangtan, 411105, PR China.

b. College of Civil Engineering, Hunan University, Changsha 410082, PR China.
c. Department of Civil and Environmental Engineering, Brunel University London, London, UB8 3PH, United Kingdom
d. International Education School, Hunan Institute of Engineering, Xiangtan, 411105, PR China.

Corresponding author: Zhi-lin LONG, College of Civil Engineering, Xiangtan University, Xiangtan, 411105, PR China. Tel: +8613617329993.

E-mail: longzl@xtu.edu.cn

Modeling the single particle crushing behavior by random discrete element method

Abstract

Microscopic properties of granular materials typically exhibit significant heterogeneity. Realistic particle crushing simulation in granular materials requires the use of model that incorporate the spatial heterogeneity of its microscopic properties. This study introduces a novel approach, the Random Field Theory-Discrete Element Method (RFT-DEM) model, to simulate the single-particle crushing behavior of granular materials, considering the spatial heterogeneity of microscopic properties within particles. The material heterogeneity was characterized through Random Field Theory, demonstrating reasonable consistency between simulated and experimental results. The size-dependent characteristics of crushing strength and Weibull modulus were confirmed through a series of single-particle crushing simulations, emphasizing the model's capability to capture such features. Systematic analyses explored the impact of coefficient of variation (COV) and scale of fluctuation (SOF) on single-particle crushing behavior. Increasing COV resulted in reduced characteristic crushing strength and Weibull modulus, with larger particles exhibiting greater sensitivity. Furthermore, increasing SOF initially increased these parameters until a threshold SOF value of 0.0005 m, beyond which they stabilized. Reduced COV or increased SOF diminished the size effect in characteristic crushing strength, and once COV exceeded a threshold of 0.03, the size effect became independent of its variations. These findings contribute to a comprehensive understanding of the intricate interplay between microscopic properties and crushing behavior in granular materials.

Key words: Discrete Element Method; Random field theory; Particle Crushing Behavior; Granular materials

1 Introduction

Crushable granular materials such as sands [1-3], coarse-grained soils [4, 5] and rock aggregates [6-8] can be found across a diverse range of civil engineering applications, from road embankments [9], rockfill dams [10, 11] to pavement structures [12]. In engineering practices, particle crushing cause alterations in the mechanical properties of granular materials, subsequently leading to a cascade of engineering problems such as the uneven settlement of foundations [13], ground instability and the reduction in the bearing capacity of drilling piles [14]. Therefore, understanding the crushing behavior of granular materials is important for the safety and stability of engineering infrastructure.

For this purpose, extensive investigations on the crushing behavior of granular materials have been carried out using various experimental approaches, including single-particle crushing tests [10, 15], triaxial shear tests [16, 17], and creep tests [18, 19]. Although the particle crushing characteristics and their correlation with the mechanical behavior can be elucidated through the aforementioned experimental approaches, it still present challenges in understanding the progressive fracturing process and fracture mechanism of crushable particles at microscopic scale [20]. Therefore, various microscopic testing approaches such as X-ray micro-computed tomography [20-22] and high-speed microscope camera [23] have been adopted to capture the microscopic crushing behavior of crushable particles. However, these approaches face challenges in their widespread application due to the constraints of costly experimental equipment. Thus, numerical approaches such as the extended finite element method (XFEM) [24-26], the material point method (MPM) [27-29], the peridynamics-based method (PDBM) [30-32], and the discrete element method (DEM) [33-35] have been developed to provide valuable insights into microscopic responses during particle breakage process, as shown in Table. 1. Among these numerical approaches, DEM has gained widespread adoption in simulating the crushing behavior of granular materials, primarily because of its remarkable capability to accurately capture multi-scale mechanical responses [36-38]. Typically, there are three DEM-based approaches for simulating the particle crushing, namely the bonded particle method [15, 39, 40], the particle replacing method [41-43] and the particle cutting method [44]. Aela et al. [45] employed the bonded particle method to acquire the fragment size distribution of individual ballast particles, and endeavored to enhance this method's computational efficiency by integrating machine learning models. Wang et al. [46] employed X-ray Computed Tomography to capture 3D images of zeolite granules during oedometer compressions. They then introduced a new replacement mode into the DEM based on the experimental results, to accurately depict the size evolution and morphology changes of zeolite granules during the breakage process. Jiménez-Herrera et al. [47] conducted a study on the effectiveness of DEM in simulating particle breakage using the bonded particle method and two different types of particle replacing method, and provided a detailed discussion on their advantages and disadvantages. Kuang et al. [44] introduced the particle cutting method to simulate the particle crushing behavior of calcareous sand under triaxial compression. They emphasized that this method ensures the conservation of mass and volume in DEM simulations. Previous research has demonstrated that all three methods mentioned above are effective in simulating particle breakage behavior. However, the pre-defined failure criterion and post-failure profile are necessary for the particle replacing and particle cutting method, rendering them inadequate for accurately modeling the crushing behavior of an individual particle [41-44]. In contrast, the bonded particle method, which models an individual crushable particle as a collection of bonded elementary balls, provides superior capabilities in simulating the multi-scale crushing behavior of an individual particle. By adopting the bonded particle method, Barbosa et al. [4] investigated the effect of soil aggregate shape on its crushing behavior and concluded that the bonded particle method can characterize the Weibullian behavior of soil aggregate with different shapes. Wang et al. [15] conducted a comprehensive discussion regarding three types contact model employed in the bonded particle method, namely, the linear bond contact model, the parallel bond contact model and the flat joint contact model. Furthermore, they explored the size effect and loading rate effect of the ballast particle crushing behavior by incorporating the flat joint contact model into the bonded particle method. These numerical investigations indicated that the brittle particle's crushing behavior is susceptible to many factors such as particle shape, size, and loading conditions. However, for natural crushable particles, the particle crushing behavior displays substantial variability, which can also be ascribed to the intrinsic heterogeneity in mineral composition and the presence of original defects at the microscopic scale [48, 49]. Based on the bonded particle DEM model, Lim et al., [50] Mcdowell et al., [51] Qian et al. [52] and Cheng et al. [53] employed a numerical method where a certain number of elementary balls were randomly removed to mimic the presence of original defects in particles, resulting in the reproduction of Weibullian behavior in particle crushing strengths. Zhou et al. [54, 55] incorporated the subcritical crack propagation theory into the bonded particle DEM model, and simulated the random crushing strength of rockfill particles by introducing random virtual cracks.

Table. 1 Comparison of numerical approaches for simulating particle breakage behavior

Numerical approaches	Main advantages and disadvantages	Application areas
XFEM [24-26]	Advantages: (a). Reduced mesh independence (b). Multi-physics coupling (c). Incorporation of complex geometries …… Disadvantages: (a). Require predefined crack tracking procedures (b). Convergence of high-order elements (c). Singularity near crack tips ……	(a). Fatigue crack growth (b). Dynamic fracture analysis (c). Analysis of crack tip behavior ……
MPM [27-29]	Advantages: (a). Handling of dynamic loading conditions (b). No need for grid reconstruction (c). Applicability to complex geometries …… Disadvantages: (a). Implementation complexity (b). Difficulty in parameter selection (c). Difficulty in handling interface behavior ……	(a). Dynamic fracture (b). High impact collision (c). Fluid-solid coupling ……
PDBM [30-32]	Advantages: (a). No need for pre-defined mesh (b). Coupling of multiple physical fields (c). Consideration of diverse crack propagation paths …… Disadvantages: (a). More parameters required (b). Huge computational cost (c). Complexity in theoretical foundation ……	(a). Fatigue fracture analysis (b). Fracture analysis of complex geometric (c). Stress-corrosion cracking ……
DEM [33-35]	Advantages: (a). Discontinuous medium modeling (b). Visualization of particle interactions (c). Incorporation of material heterogeneity …… Disadvantages: (a). Huge computational cost (b). Sensitivity to model parameters (c). Challenges in simulating large-scale systems ……	(a). Particle breakage under complex loading conditions (b). Influence of particle breakage on material mechanical properties (c). Numerical model improvements for particle breakage ……

Although the above-mentioned approaches have been proven effective in capturing the variability of particle crushing strength, the spatial variability in microscopic properties is still neglected. To account for this, previous studies [29, 56, 57] have utilized bonding strength parameters that follow a Normal or Gaussian distribution to create heterogeneous numerical particles with probabilistic microscopic properties. By employing this approach, the variability in overall particle crushing strength can also be effectively replicated by the bonded particle DEM model. Nonetheless, the statistical distributions are insufficient to adequately characterize the microscopic uncertainties because the microscopic properties in geomaterials vary spatially with a higher similarity at neighboring locations than that at distantly locations [58]. Recently, some novel DEM-based approaches have been developed to simulate random microscopic material properties through the application of random field theory (RFT) which has been demonstrated as an effective approach to adequately characterize the spatial variability of geomaterial properties [59-62]. For instance, Nie et al. [59] simulated the heterogeneity of particle properties of sandy soil by incorporating the RFT into DEM, and conducted a comprehensive analysis of its multi-scale mechanical responses. Zhao et al. [61] and Li et al. [62] employed the random discrete element method to simulate the heterogeneity of rock, and further investigated its fragmentation mechanism. Aforementioned, the variability in single particle crushing strength of granular materials can be attributed to their uncertainties associated with their microscopic properties [48, 49], and hence the incorporation of RFT into DEM could be an appropriate option for a comprehensive understanding of its multi-scale crushing behavior.

This work endeavors to model the single particle crushing behavior of granular materials using the bonded particle DEM model incorporating the spatial inhomogeneous microscopic properties within particles. Firstly, an RFT-DEM model was developed to simulate the spatial heterogeneity of individual sand particle by integrating RFT into DEM. The proposed RFT-DEM model utilized the bonded particle method to create individual particles in DEM, based on the parallel bond contact model. Additionally, the heterogeneity of microscopic properties within particles was characterized by a random field for four strength parameters in parallel bonds, including effective modulus, critical tensile strength, cohesion, and friction angle. The RFT-DEM model was further validated and calibrated against the crushing strength data of quartz sand particles reported in Nakata et al. [63]. Subsequently, the RFT-DEM model has been employed to analyze the size-dependent particle crushing strength and its mechanism. And finally, A further parametric study on the effect of coefficient of variation (COV) and scale of fluctuation (SOF) on single particle crushing behavior has also been performed.

2 Methodology and model configuration

2.1 DEM model

The bonded particle DEM model has been extensively adopted to simulate the crushing behavior of brittle particles such as calcareous sand particles [64], quartz sand particles [65], and ceramic particles [66]. In the bonded particle DEM model, the numerical sample is modelled as a series of bonded elementary balls, and the contact interactions between two elementary balls are transmitted through the parallel bond contact, as shown in Fig. 1.

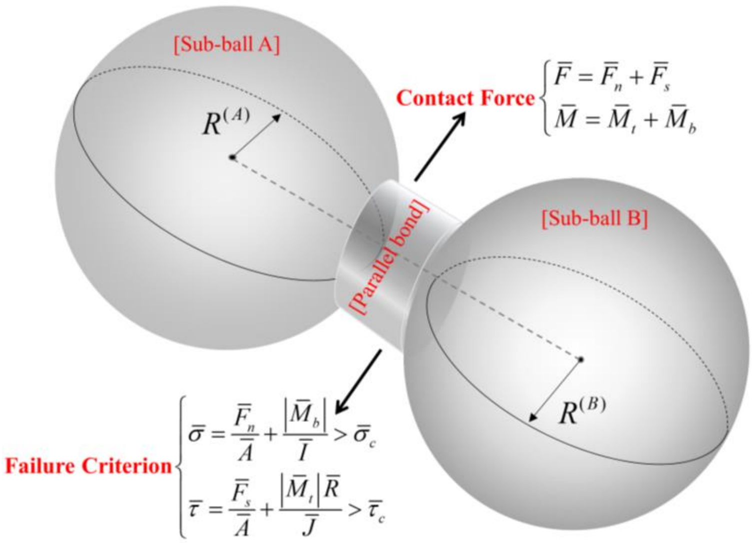

Fig. 1 Parallel bond contact behavior

For two contacting sub-balls bonded by the parallel bond model, the normal ($\Delta\bar{F}_n$) and shear ($\Delta\bar{F}_s$) contact force can be calculated incrementally as:

$$\Delta\bar{F}_n = -\bar{k}_n \bar{A} \Delta U_n, \quad \Delta\bar{F}_s = -\bar{k}_s \bar{A} \Delta U_s \tag{1}$$

where $\bar{k}_n$ and $\bar{k}_s$ are the parallel-bond normal and shear contact stiffness, ΔU_n and ΔU_s are the incremental displacements between two bonded sub-balls in the normal and shear directions. For the parallel bond contact model, the parallel-bond contact stiffness can be calculated by the parallel-bond effective modulus

($\bar{E}$) and the parallel-bond stiffness ratio ($\bar{k}_r$):

$$\bar{k}_n = \frac{\bar{A}\cdot\bar{E}}{\bar{L}}, \quad \bar{k}_s = \frac{\bar{k}_n}{\bar{k}_r}, \quad \text{with} \begin{cases} L = \begin{cases} R^{[A]} + R^{[B]}, & ball-ball \\ R^{[A]}, & ball-facet \end{cases} \\ \bar{A} = \pi\bar{R}^2, \text{ with } \bar{R} = \begin{cases} \min(R^{[A]} + R^{[B]}), & ball-ball \\ R^{[A]}, & ball-facet \end{cases} \end{cases} \tag{2}$$

In addition, the parallel bond between two sub-balls can also transmit moments. According to the incremental twisting ($\Delta\theta_t$) and bending ($\Delta\theta_b$) rotation angle in one computation cycle, the corresponding increment of twisting ($\Delta\bar{M}_t$) and bending ($\Delta\bar{M}_b$) moments can be calculated by:

$$\Delta\bar{M}_t = -\bar{k}_s\bar{J}\Delta\theta_t, \quad \Delta\bar{M}_b = -\bar{k}_n\bar{I}\Delta\theta_b \tag{3}$$

where $\bar{I}$ and $\bar{J}$ are the moment and polar moment of inertia, respectively.

Once the current tensile ($\bar{\sigma}$) or shear ($\bar{\tau}$) stress of the parallel-bond exceeds the critical tensile ($\bar{\sigma}_c$) or shear ($\bar{\tau}_c$) strength, the parallel bond contact between two sub-balls is removed and instantaneously replaced by the linear contact. During the DEM calculation process, the critical shear strength ($\bar{\tau}_c$) is constantly updated according to $\bar{\tau}_c = \bar{c} - \bar{\sigma}\tan\bar{\phi}$ with $\bar{c}$ being the cohesion and $\bar{\phi}$ being the parallel-bond friction angle. The failure criterion of parallel bonds is as follows:

$$\bar{\sigma} = \frac{\bar{F}_n}{\bar{A}} + \frac{|\bar{M}_b|\bar{R}}{\bar{I}} > \bar{\sigma}_c \tag{4}$$

$$\bar{\tau} = \frac{\bar{F}_s}{\bar{A}} + \frac{|\bar{M}_t|\bar{R}}{\bar{J}} > \bar{\tau}_c = \bar{c} - \bar{\sigma}\tan\bar{\phi} \tag{5}$$

After the parallel-bond between two sub-balls is removed, the contact force can then be calculated by using the linear contact model:

$$F_n = k_n U_n \tag{6}$$

$$\Delta F_s = -k_s \Delta U_s \tag{7}$$

where k_n and k_s are the linear contact stiffness in normal and shear directions, which can also be obtained by the Eq.(2) according to the linear effective modulus (E) and the parallel-bond stiffness ratio (k_r). Besides, the magnitude of shear force ($F_s^{\max}$) between two unbonded sub-balls is limited by $F_s^{\max} = \mu|F_n|$ with μ being the friction coefficient.

2.2 Random field theory

Natural geomaterials typically exhibit a significant inherent spatial variability in their physical and mechanical properties. This variability stems from a range of complex factors, including stress history, joints weathering, geological transport and deposition processes [67, 68, 82]. Since then, in this study, the integration of RFT and DEM has been employed to characterize the intrinsic heterogeneity within individual sand particles, thereby enabling an accurate reproducing of its single particle crushing behavior. In RFT, the autocorrelation function is adopted to describe the correlation between random properties at any two points in the spatial space. Typically, researchers often resort to employing various theoretical autocorrelation functions such as the exponential function [69], the triangular function [58], and the Gaussian function [60]. This is primarily motivated by the challenge of obtaining an exact autocorrelation function based on the limited data from in-situ tests. Among these theoretical autocorrelation functions, the Gaussian autocorrelation function often preferred due to its ability to more accurately capture the spatial variability inherent in geomaterial properties [70]. Therefore, the Gaussian autocorrelation function is adopted in this study, and the autocorrelation coefficient (ρ_{ij}) for a specific geomaterial property between i^{th} and j^{th} element can be calculated as:

$$\rho_{ij}\left(\Delta_{x,ij},\Delta_{y,ij},\Delta_{z,ij}\right)=\exp\left[-\pi\left(\left(\frac{\Delta_{x,ij}}{\delta_x}\right)^2+\left(\frac{\Delta_{y,ij}}{\delta_y}\right)^2+\left(\frac{\Delta_{z,ij}}{\delta_z}\right)^2\right)\right]\quad i,j=1,2,3,......,n \tag{8}$$

where $\Delta_{x,ij}$, $\Delta_{y,ij}$ and $\Delta_{z,ij}$ are the distances between i^{th} and j^{th} element along the x- , y- and z- axis, respectively. n is the total number of elements. δ_x , δ_y and δ_z are the scale of fluctuation (SOF) of the specific property *k*. The SOF stands for the correlation length, within which the random properties exhibit a strong correlation. In this study, the same value is assigned to the SOF in three different directions. Subsequently, the standard normal random field $N(x, y, z)$ is accessed by:

$$N(x,y,z)=LU \tag{9}$$

where L is a lower triangular matrix calculated by the Cholesky decomposition in the equation $\rho=LL^T$ with ρ being the autocorrelation matrix. U represents an *n*-dimensional column vector that follows a standard normal distribution. Following Eq.(10), a lognormal random filed of the specific property *k* can then be generated according to the mean value ($\sigma_{\ln k}$) and standard deviation ($\mu_{\ln k}$) of the normal distribution of $\ln(k)$:

$$k(x,y,z)=\exp\left[\mu_{\ln k}+\sigma_{\ln k}\cdot N(x,y,z)\right] \quad with \begin{cases} \sigma_{\ln k}=\sqrt{\ln\left(1+\mathrm{COV}_k^2\right)} \\ \mu_{\ln k}=\ln\mu_k-\frac{1}{2}\sigma_{\ln k}^2 \end{cases} \tag{10}$$

where μ_k and COV_k represent the mean value and coefficient of variation (COV) of the specific property *k*, respectively.

2.3 Model configuration of single particle crushing tests

Single particle crushing test is further adopted to explore the particle crushing behavior of granular materials with a random micro-properties. The model configuration of single particle crushing test has been developed by incorporating RFT into DEM, whose flowchart is shown in Fig. 2. Firstly, an assembly of 28844 elementary spherical balls whose radius ranged from 0.03 mm to 0.04 mm are generated with a cubic domain with a side length of 2 mm. Further, elementary balls are bonded by parallel bonds with constant parameters to form the homogeneous cubic sample. Then, a series of random parameter values of parallel bonds are generated based on the RFT, and subsequently reassigned to the sample. In this work, following the suggestions given by Zhao et al. [61] and Zhang et al. [29], four strength parameters in parallel bonds namely effective modulus ($\bar{E}$), critical tensile strength ($\bar{\sigma}_c$), cohesion ($\bar{c}$) and friction angle ($\bar{\phi}$) are set as random values. The individual particle sample with a specific diameter is generated by removing the elementary balls that fall outside of its range. Subsequently, single particle crushing tests can be conducted on the individual particle sample. In the test, the loading plates are modelled by two rigid walls, and the top wall is moved down with a constant axial velocity until failure.

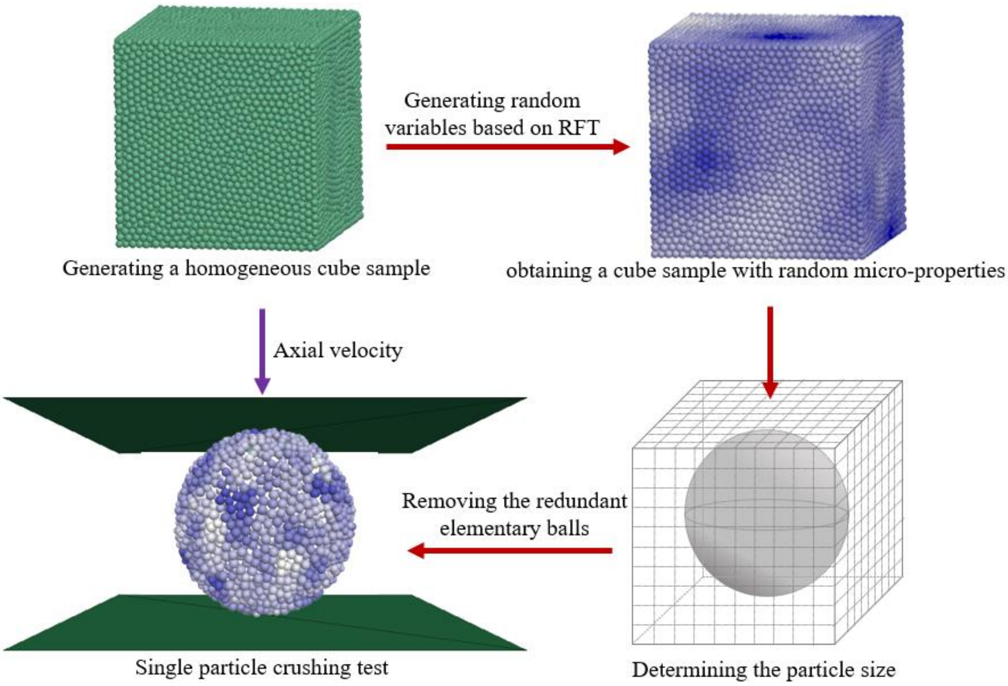

Fig. 2 Model configuration of single particle crushing tests

This study attempts to comprehensively investigate the variability of particle breakage behavior and its size-dependency by adopting the RFT-DEM model. Hence, individual particle samples with different sizes were generated by using the sample preparation procedure and presented in Fig. 2. Furthermore, the effects of statistical parameters in RFT (COV and SOF) on particle breakage behavior were also examined, with the objective of gaining a detailed microscopic understanding of size effect in crushable particles. The typical random filed with different values of COV and SOF generated for the various-sized particle samples are illustrated in Fig. 3. The material coefficient for the elementary balls is defined as the ratio between the exact value and the mean value of micro-parameters in parallel bonds. From Fig. 3, it can be seen that the integration of the RFT into the DEM can effectively simulate the variability in the micro-properties of individual particles. In addition, the particle samples with smaller sizes display a greater heterogeneity in the micro-properties. In the case of a specific SOF, the particle samples become more homogeneous with the decrease in the COV. For a COV of 1.0, the material coefficient for elementary balls ranges from 22.8920 to 0.0008. It is also obvious that the distribution of the material coefficient within the particle is significantly inhomogeneous. When the COV decreases to 0.003, the maximum and minimum material coefficients for elementary balls are very close, at 1.0166 and 0.9852 respectively. Especially, the material coefficient for all elementary balls is almost equal to 1.0 while the COV is 0.001, indicating a significant homogeneity in the micro-properties within the particle samples. Besides, a more homogeneous particle sample can be created by increasing the SOF while maintaining a constant COV of 0.3, as depicted in Fig. 3(b). When the SOF is 0.00005 m, the material coefficient for elementary balls ranges from 5.9056 to 0.1368. As the SOF increases, the distribution range of the material coefficient gradually decreases. When the SOF value increases to 0.005 m, further increases in the SOF value have a minor impact on the material coefficient. This finding has been corroborated by the observations made in Li et al. [62] and Nie et al. [59] which demonstrated that a random field generated with a sufficiently large SOF could remain entirely constant.

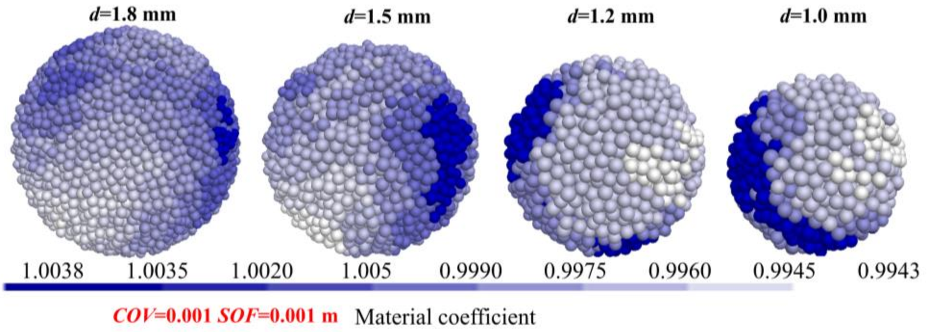

(a-1) *COV*=0.001 and *SOF*=0.001 m

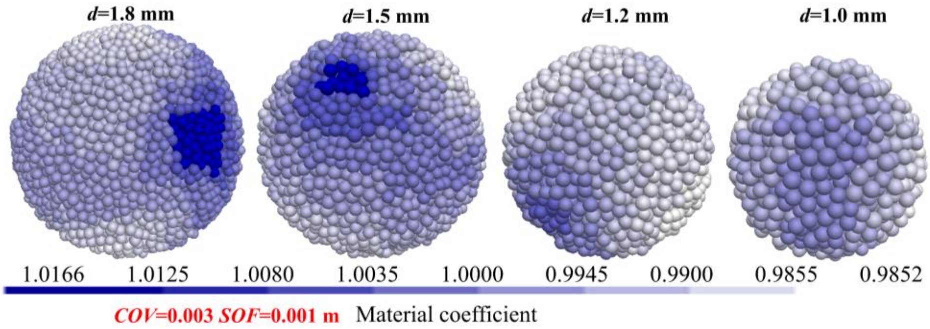

(a-2) *COV*=0.003 and *SOF*=0.001 m

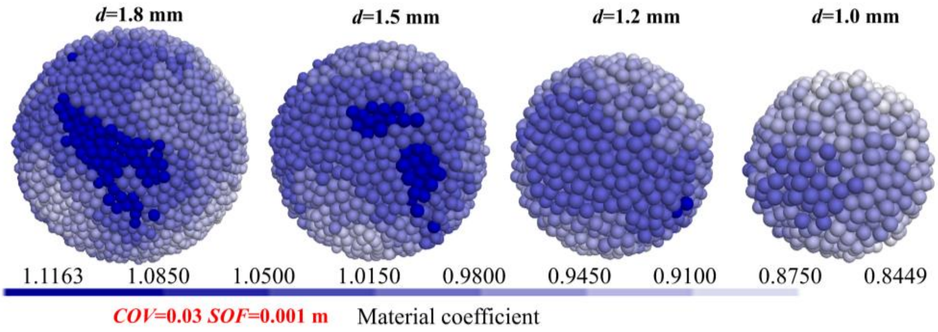

(a-3) *COV*=0.03 and *SOF*=0.001 m

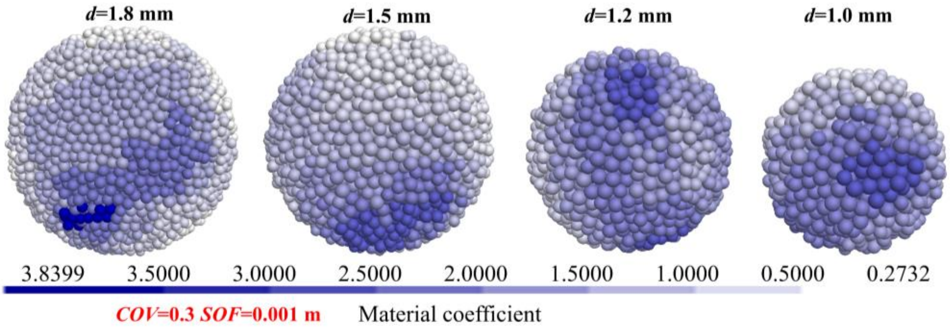

(a-4) *COV*=0.3 and *SOF*=0.001 m

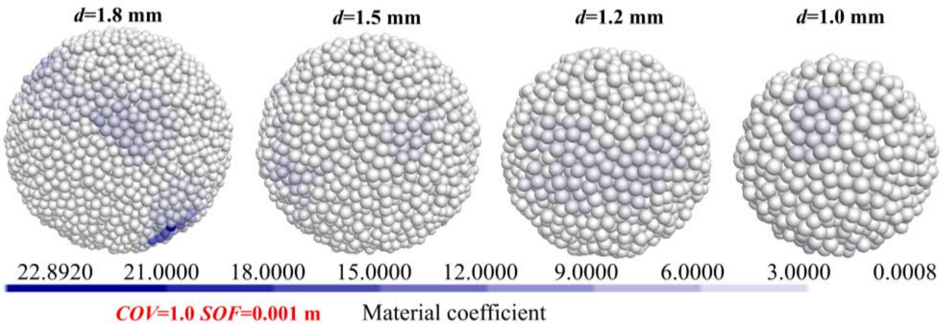

(a-5) *COV*=1.0 and *SOF*=0.001 m

(a)

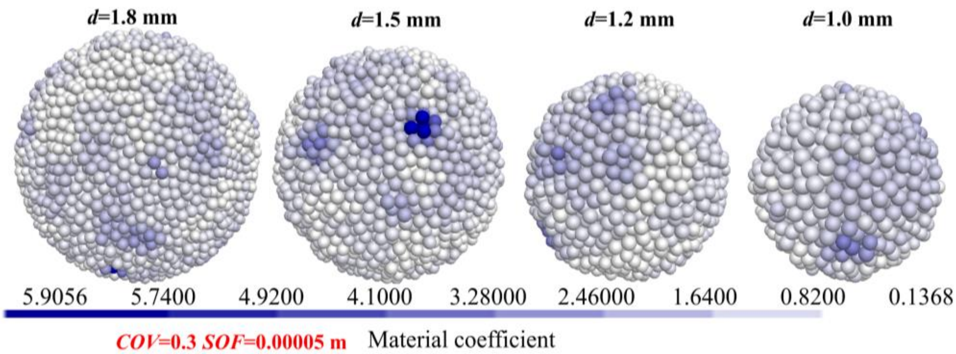

(b-1) *COV*=0.3 and *SOF*=0.00005 m

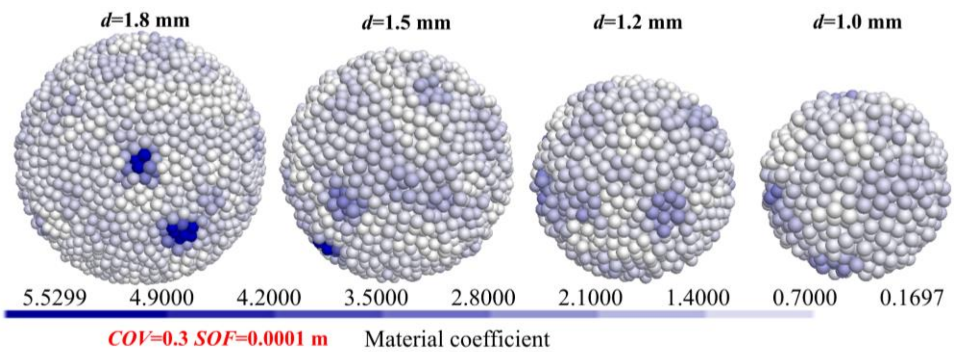

(b-2) *COV*=0.3 and *SOF*=0.0001 m

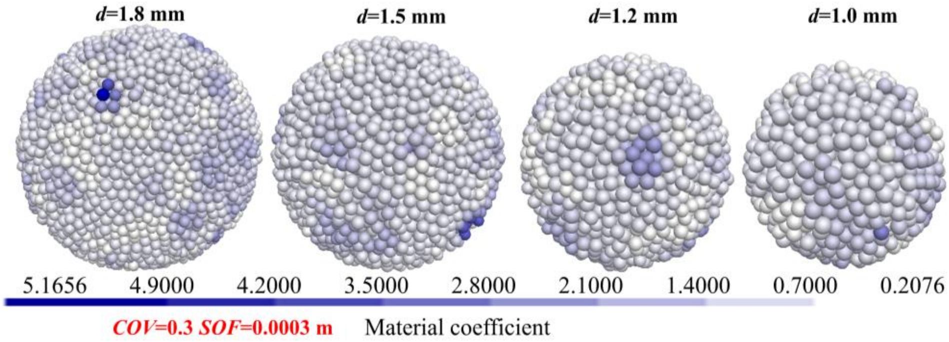

(b-3) *COV*=0.3 and *SOF*=0.0003 m

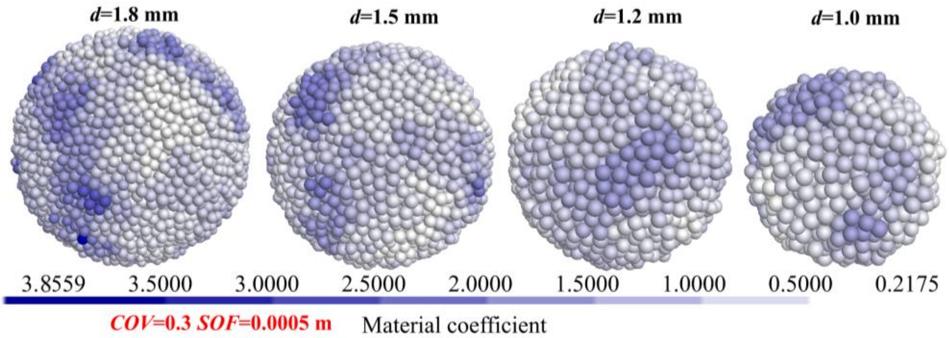

(b-4) *COV*=0.3 and *SOF*=0.0005 m

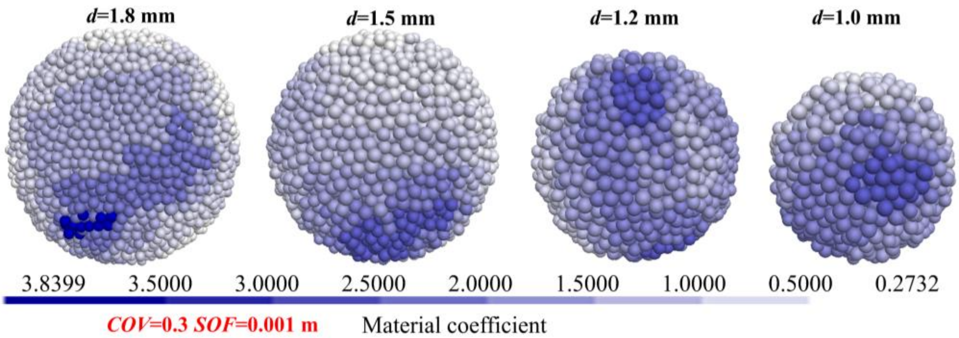

(b-5) *COV*=0.3 and *SOF*=0.001 m

(b)

Fig. 3 Typical random field for various-sized particle samples: (a) under different *COV* with *SOF*=0.001 m (b) under different *SOF* with *COV*=0.3

For a more intuitive observation of the impact of COV and SOF values on material coefficient in particle samples, typical cumulative frequency of material coefficient in particle samples with a diameter of 1.0 mm are presented in Fig. 4. It is further evident that the COV values significantly influence the material coefficient in particle samples. When the COV is set at 0.3 or 1.0, there is an obvious non-uniformity observed in the material coefficient, accompanied by a wide distribution range. However, as the COV decreases below 0.03, material coefficients predominantly converge toward 1.0. Furthermore, when compared to COV values, the effect of SOF values on material coefficient is less obvious.

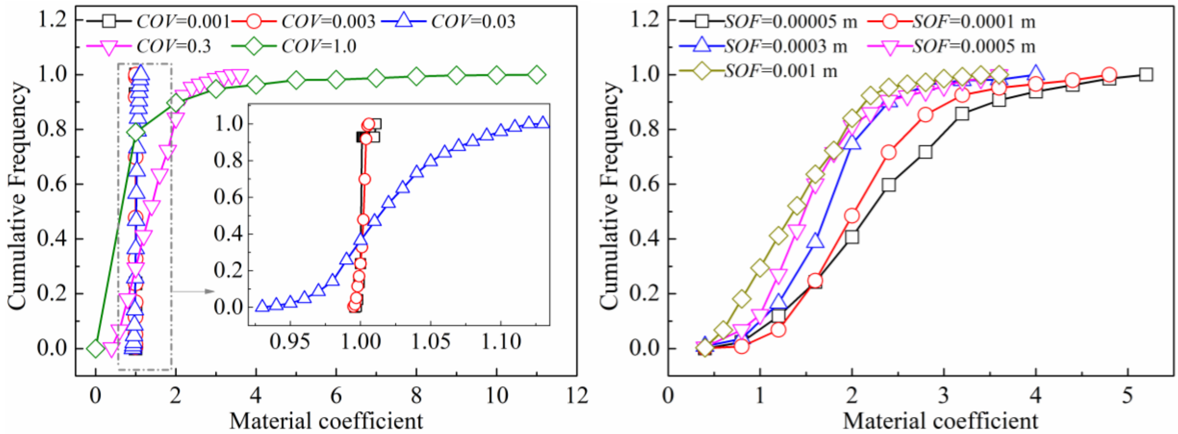

(a) (b)

Fig. 4 Typical cumulative frequency of material coefficient in particle samples with a diameter of 1.0 mm: (a) under different *COV* with *SOF*=0.001 m (b) under different *SOF* with *COV*=0.3

3 Numerical Results

3.1 Variability in single particle crushing strength

In single particle crushing tests, the particle crushing strength σ can be determined using the following equation:

$$\sigma = \frac{F_p}{d_p^{\ 2}} \tag{11}$$

where F_p stands for the applied axial force at failure, and d_p is the particle diameter.

Even if the particles have the identical size, the crushing strength for each particle exhibits variability due to the inherent diversity in micro-properties [48, 49]. Therefore, some probabilistic statistical models were adopted to characterize the great randomness in particle crushing strength [71-73]. Among these proposed models, the Weibull model based on the weakest-link theory is preferred as it provides an excellent ability in evaluating particle crushing strength, which has been confirmed by numerous investigations [29, 30, 49-52]. In Weibull model, the following distribution rule with two statistical parameters, namely characteristic crushing strength (σ_c) and Weibull modulus (m), are used to characterize the particle crushing strength:

$$P_s = \exp\left[-\left(\frac{\sigma}{\sigma_c}\right)^m\right] \tag{12}$$

where P_s is the survival probability and can be calculated as $P_s = 1 - N_c/(N_t + 1)$ where N_c denotes the number of crushed particles under a applied tensile stress of σ and N_c denotes the total number of tested particles. The characteristic crushing strength (σ_c) is approximately equal to the mean value of particle crushing strength [50], and it can be determined as the value of the applied tensile stress when $P_s = 37\%$. Additionally, the Weibull modulus (m) is recognized as a pivotal parameter governing the variation of particle crushing strength, and a larger value of m indicates a smaller variation of particle crushing strength.

In order to conveniently calculate the characteristic crushing strength and Weibull modulus, Eq.(12) is typically rewritten in a linear form:

$$\ln\left[\ln\left(\frac{1}{P_s}\right)\right] = m\ln\left(\frac{\sigma}{\sigma_c}\right) \tag{13}$$

The microscopic parameters used in the proposed RFT-DEM model are first calibrated to match the crushing strength of quartz sand particles with diameters ranged from 1.0 to 1.18 mm as described in Nakata et al. [63]. In the experiments, a displacement-controlled particle-crushing apparatus with a load capacity of 500 N and a resolution of 0.01 N was utilized. The targeted quartz sand particle was placed between two loading platens. Then, the bottom loading platen was moved at an axial velocity of 0.1 mm/min, while the top loading platen stayed in a fixed position. The axial force and displacement were continuously measured during the loading process. During the model calibration, the diameter of numerical particles is set to a specific value of 1.18 mm, while an axial velocity of 0.1 mm/min is carefully selected to maintain consistency with experimental conditions. It is difficult to determine the reasonable microscopic parameters for DEM model since they cannot be directly obtained through experimental measurements or theoretical analysis [74]. Hence, a trial-and-error calibration procedure is often employed to determine the DEM model parameters. After a series of trials, the model parameters are identified and shown in Table. 2.

Table. 2 RFT-DEM model parameters

Parameter description	Values
Mean bond effective modulus, $\bar{E}$, [Pa]	7.0×10^8
Mean bond critical tensile strength, $\bar{\sigma}_c$, [Pa]	4.5×10^7
Mean bond cohesion, $\bar{c}$, [Pa]	4.5×10^7
Mean bond friction angle, $\bar{\phi}$, [。]	30
Bond stiffness ratio, $\bar{k}_r$, [--]	1.0
Ball effective modulus, E, [Pa]	2.0×10^9

Ball stiffness ratio, k_r, [--]	1.0
Ball friction coefficient, μ, [--]	0.577
Ball Density, ρ, [kg/m^3]	2650
Damping coefficient, β, [--]	0.5
Coefficient of variation, *COV*, [--]	0.3
Scale of fluctuation, *SOF*, [m]	0.001

A series of single particle crushing simulations have been performed by adopting the above RFT-DEM model parameters. Based on the Weibull model, the comparison of particle survival probabilities between the simulations and experiments is illustrated in Fig. 5. The simulations results reveal a great variability in particle crushing strength, in line with the experimental findings. Besides, both the simulations and experiments results can match the theoretical Weibull model, as shown in Fig. 5(b), implying that the integration of RFT and DEM can provide statistical variability of particle crushing strength. Furthermore, the values of σ_c for simulation and experiment are 47.92 and 46.37, respectively, while the corresponding values of m are 2.62 and 2.45, respectively. A larger Weibull modulus in simulations suggests a slightly smaller variability of crushing strength compared to that observed in experiments, which is primarily attributed to the inherent limitations of simulations in fully reproducing the size and shape variations of individual particles in experiments. Additionally, both the R^2 for experiment and simulation results are smaller than 0.9. Specifically, the lower crushing strength deviates more from the Weibull behavior. This is attributed to a minimum crushing stress, below which the particle will not break [75, 76].

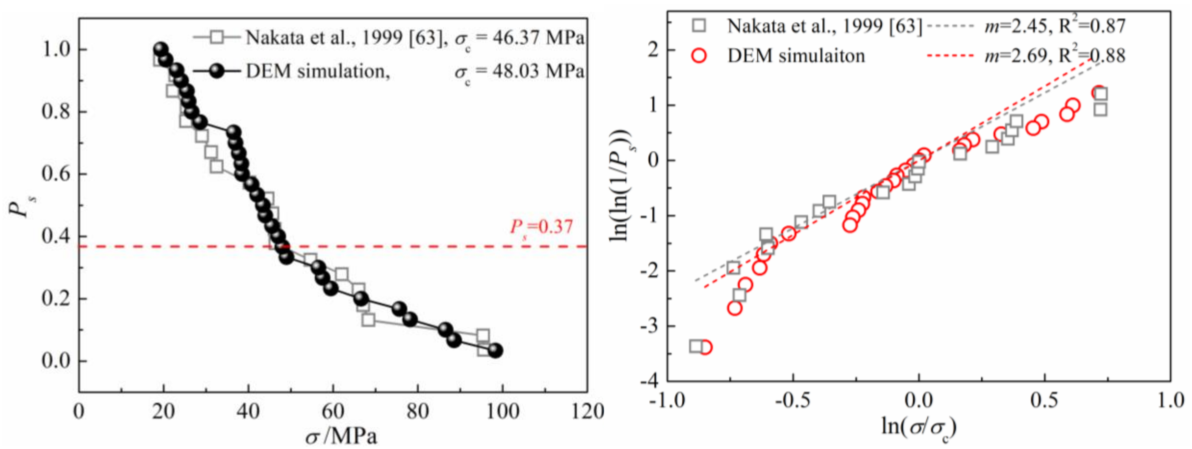

(a) (b)

Fig. 5 Comparison of numerical and experimental particle crushing strength: (a) Survival probability; (b) Weibull distribution

3.2 Size effect of single particle crushing strength

The particle crushing strength of natural brittle particles often exhibits a size-dependent behavior, and this behavior is believed to result from the spatial heterogeneity of microscopic properties [27, 30, 36, 48, 49]. A series of single particle crushing simulations were conducted on four particle groups of varying sizes using the proposed RFT-DEM model. Fig. 6 presents the crushing strength distribution of particles with different sizes. It can be observed that both the particle crushing strength and its variability shows significant size-dependent behavior. The values of *m* for numerical particles with particle sizes of 1.0 mm, 1.2 mm, 1.5 mm and 1.8 mm are 2.79, 2.62, 2.53 and 2.52, respectively. It seems that a larger particle size can result in a larger Weibull modulus, corresponding to a greater variability in crushing strength. Meanwhile, the relationship between the characteristic crushing strength and particle size is compared with the experimental results in Nakata et al., as shown in Fig. 6(c). Regarding the numerical results, size-dependent particle crushing strength is approximately linear on a double logarithmic scale, suggesting that a similar trend is consistent with the experimental results. These observations indicate that the RFT-DEM model is capable of capturing the size-dependent particle crushing behavior.

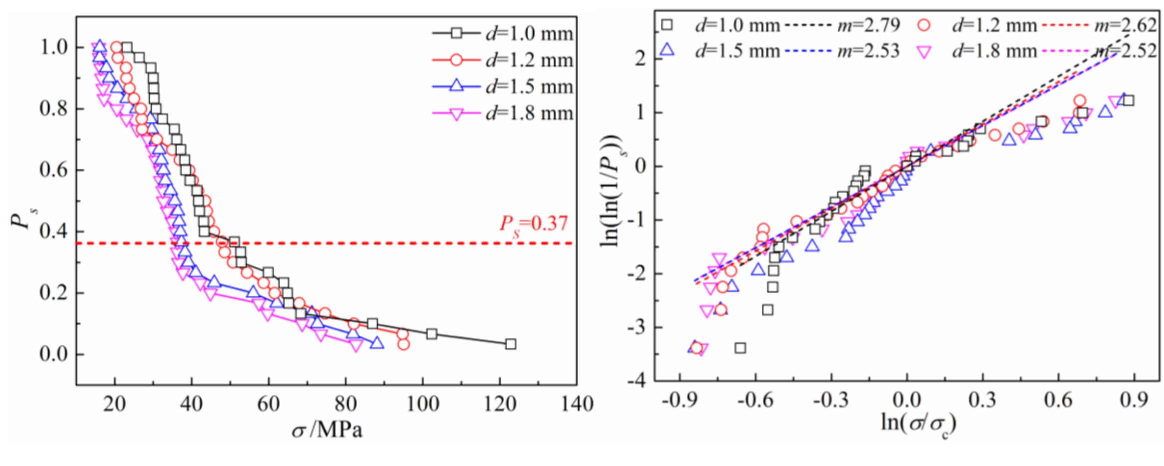

(a) (b)

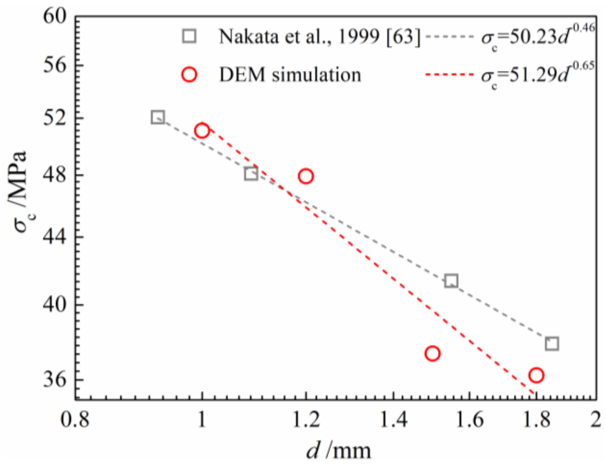

(c)

Fig. 6 Crushing strength distributions of particles with different sizes: (a) Survival probability; (b) Weibull distribution; (c) Size effect of particle crushing strength

The typical statistics of material coefficients for numerical particles of different sizes are illustrated in Fig. 7. The material coefficients for particle of different sizes all follow the lognormal distribution. The percentage of "weak" and "strong" zones for numerical particles with different initial sizes may be further analyzed to improve understanding of the size effect at microscopic scale. Here, the "weak" zone denotes the elementary balls whose microscopic strength parameters in parallel bonds are smaller than the specific mean value, i.e., the corresponding material coefficient is less than or equal to 1.0. Conversely, the "strong" zone denotes the elementary balls with a material coefficient greater than 1.0. The percentage of weak zones for particle sizes of 1.0 mm, 1.2 mm, 1.5 mm and 1.8 mm are 0.014, 0.043, 0.083 and 0.096, respectively, and the corresponding cumulative counts of weak zones are 27, 143, 679 and 1828. Under the action of the load, localized stress concentrations may readily develop at weak zones, resulting in the initiation and propagation of local cracks [71, 72]. The larger particles contain more weak zones, leading to a higher probability of crack initiation and propagation that will promote particle breakage. Hence, the size effect on particle crushing strength could be believed to be primarily attributed to the cumulative counts of weak regions, consistent with the statement that the larger particle has a smaller crushing strength because it contains more flaws [48, 49]. Additionally, the mean value of material coefficients for particle sizes of 1.0 mm, 1.2 mm, 1.5 mm and 1.8 mm are 1.84, 1.84, 1.80 and 1.70, respectively, which further strengthens the observation that there is a negative relationship between particle size and crushing strength. Moreover, it also can be observed that COV of material coefficient increases as particle sizes increase, suggesting that larger particles have less homogeneous microscopic properties, resulting in greater variability in their crushing strength.

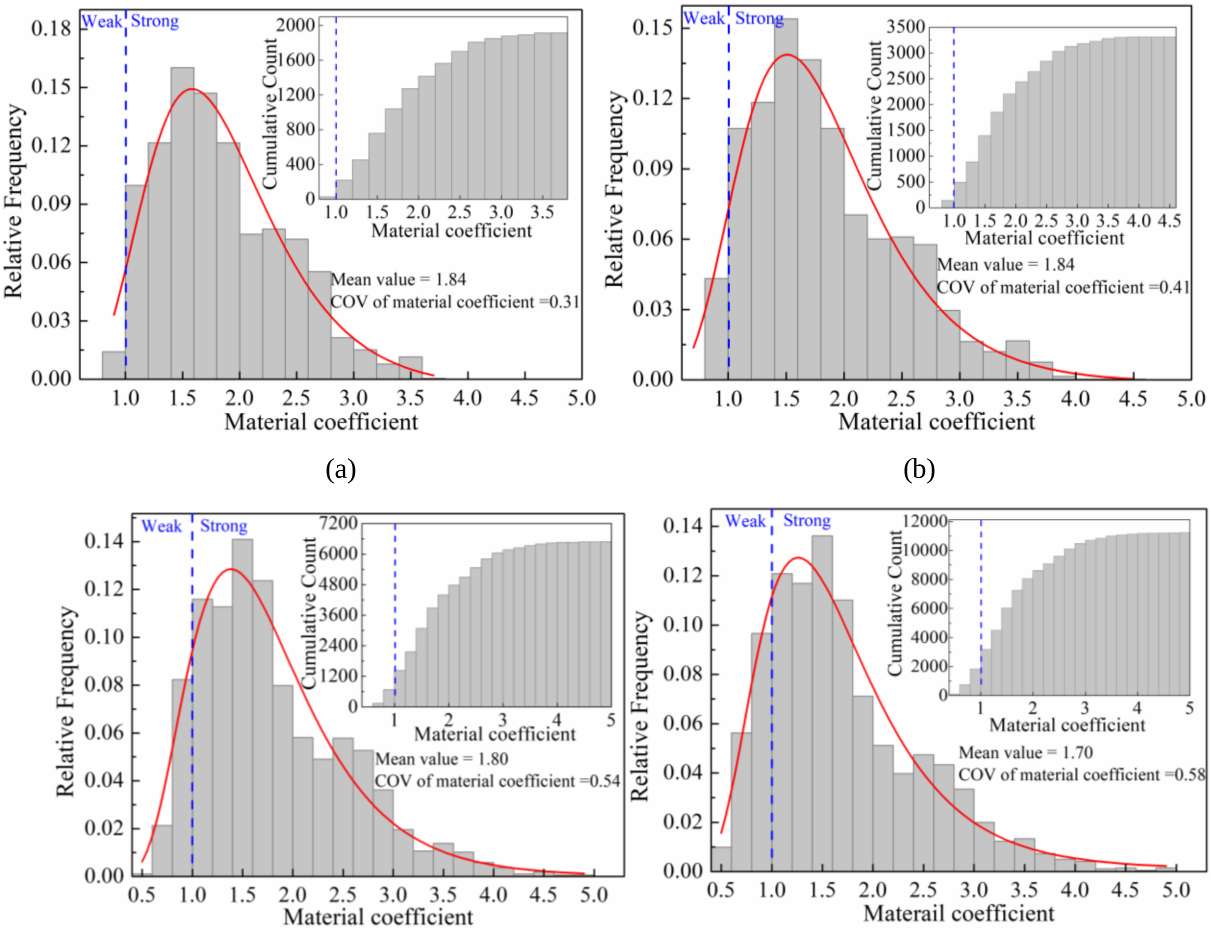

(a) (b) (c) (d)

Fig. 7 Typical statistics of material coefficients for numerical particles with various sizes: (a) d=1.0 mm; (b) d=1.2 mm; (c) d=1.5 mm; (d) d=1.8 mm

3.3 Effect of coefficient of variation on single particle crushing behavior

In the RFT-DEM model, two statistical parameters, namely COV and SOF, significantly affect the statistics of microscopic properties. To further elucidate the correlation the random field and the single particle crushing behavior, an in-depth analysis has been conducted on the effect of COV and SOF on the crushing behavior of individual particles. First, a series of single particle crushing simulations are performed on numerical particles of varying sizes, with their microscopic properties being generated by a random field. The COV values range from 0.001 to 1.0, while a constant SOF value of 0.001 m is maintained. The resulting distribution of crushing strength is visually depicted d in Fig. 8. Across all scenarios, the particle crushing strength displays variability and closely adheres to the Weibull distribution. Additionally, the size effect of crushing strength can also be accurately captured. However, it is important to note that the Weibull modulus is significantly large for scenarios with a COV value smaller than 0.03, i.e., the apparent homogeneity of the corresponding numerical particles.

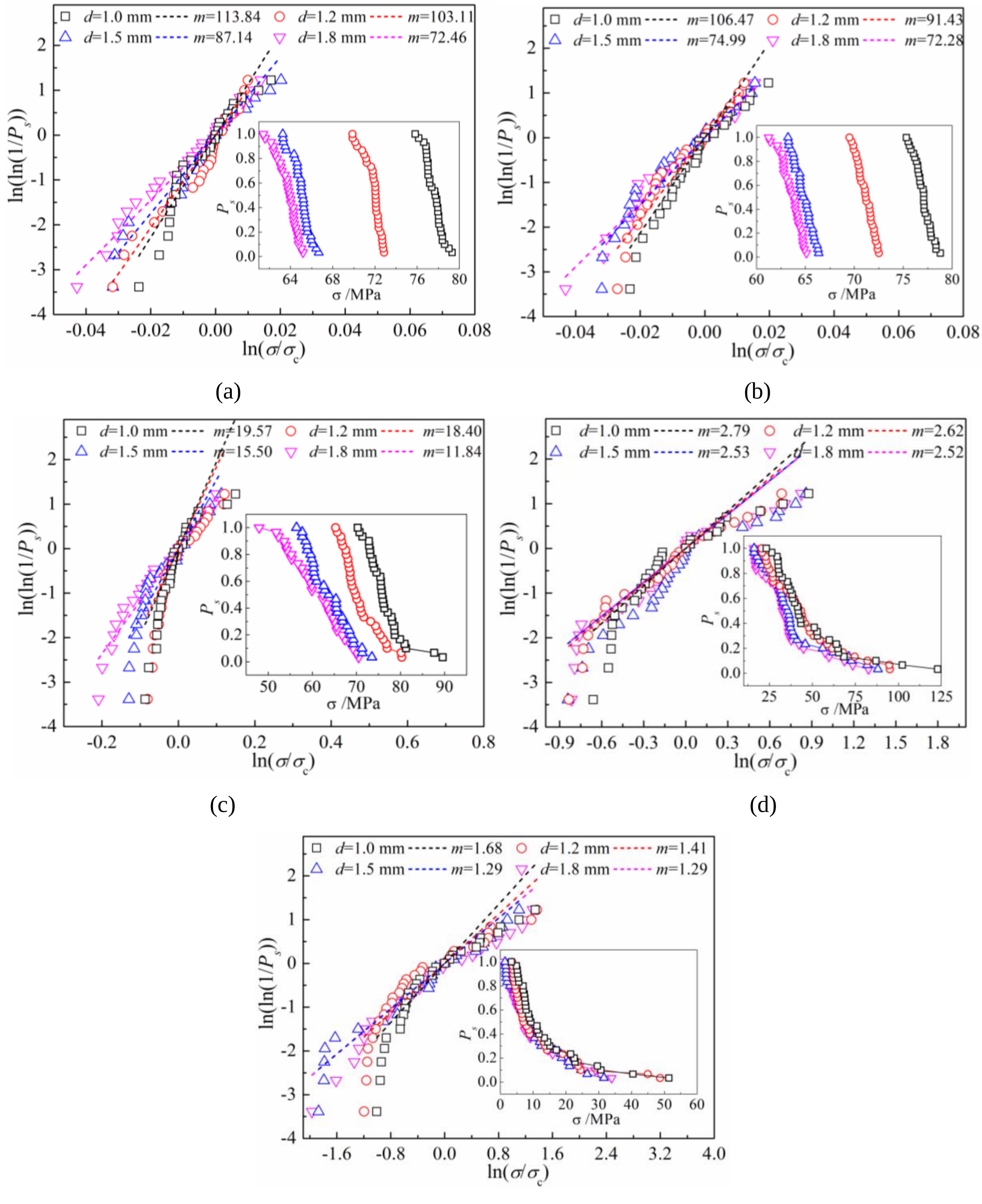

Fig. 8 Crushing strength distribution for numerical particles with random microscopic properties modelled by

the RFT with different values of *COV*: (a) *COV*=0.001; (b) *COV*=0.003; (c) *COV*=0.03; (d) *COV*=0.3; (e) *COV*=1

The relationships between Weibull parameters and COV values are plotted in Fig. 9. Both the characteristic crushing strength and the Weibull modulus often decrease with the increasing value of COV. Generally, a larger value of COV indicates that the microscopic properties of numerical particles exhibit greater variability, resulting in a smaller Weibull modulus. Meanwhile, the presence of more weak zones within the numerical particles contributes to a reduction in particle crushing strength. In addition, the characteristic crushing strength and the Weibull modulus of the larger numerical particles is more sensitive to the value of COV than that of the small particles. Such behavior is consistent with the findings made by Syroka-Koro et al. [77] that the larger the sample size, the stronger the effect of COV values on both the mean value and variability of macroscopic responses of concrete beams. The random filed realizations depicted in Fig. 3(a) provide compelling evidence that the variability of microscopic properties in larger numerical particles is more sensitive to the COV values when compared to their smaller counterparts.

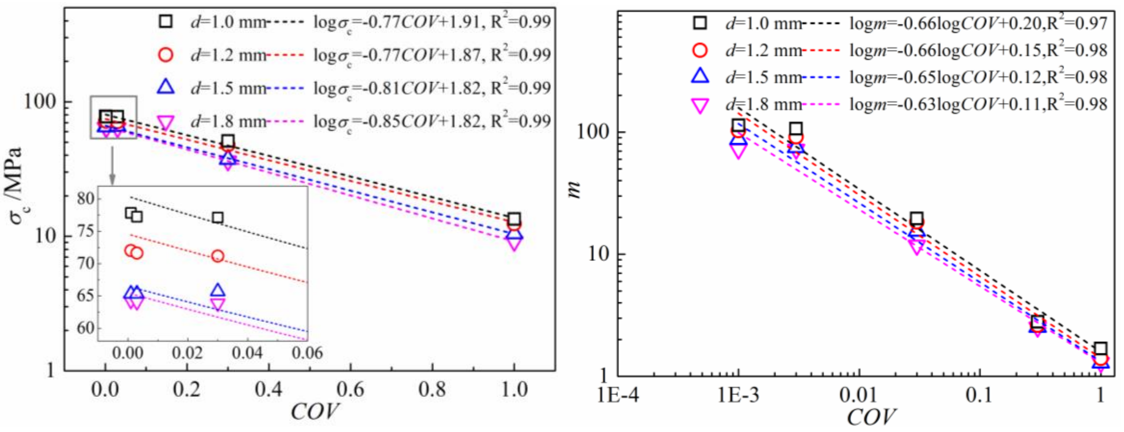

(a) (b)

Fig. 9 Weibull parameters versus *COV* values: (a) Characteristic crushing strength; (b) Weibull modulus

Fig. 10 illustrates the effect of *COV* values on the size effect. It can be observed that the size effect becomes more obvious as the value of *COV* increases. Furthermore, it is worth mentioning that the slope value of the fitting lines remains consistently at -0.33 when the value of *COV* is smaller than or equal to 0.03, indicating that the variability of microscopic properties for numerical particles remains almost unchanged within this range of *COV* values. Based on the random field realizations illustrated in Fig. 3(a), it is found that when the value of *COV* is smaller than or equal to 0.03, the maximum and minimum values of the material coefficient for numerical particle with different sizes are extremely close to each other, with both approaching 1.0, resulting in a weak size effect in particle crushing strength.

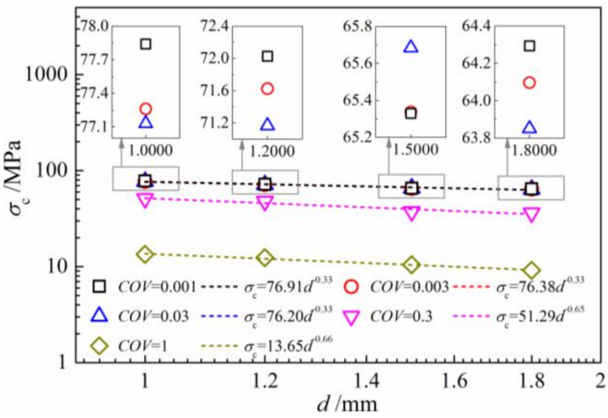

Fig. 10 The effect of *COV* values on the size effect

3.4 Effect of scale of fluctuation on single particle crushing behavior

Apart from the COV, the SOF is also pivotal in elucidating the spatial variability of a random field. Although the values of SOF for geotechnical system can be estimated approximately using various methods such as the autocorrelation function method [59], semivariogram function method [58], time series analysis [78, 79], and local average theory [80, 81], it remains challenging to determine the SOF value for an individual particle due to the lack of specific data requirements regarding microscopic properties that can only be measured by experiments. Here a parametric study is performed to investigate the effect of SOF values on particle crushing behavior, which may potentially offer valuable insights into the estimation of SOF for an individual particle. To analyze the sensitivity of particle crushing behavior to the values of SOF, a range of 0.00005 m to 0.001 m is considered, while maintaining a constant COV value of 0.3. Fig. 11 presents the crushing strength distribution for numerical particles with random microscopic properties modelled by random fields with different values of SOF. All the random field realizations with different values of SOF can ensure the variability in microscopic properties, which is evident from the fact that the crushing strength of numerical particles all conforms to the Weibull distribution. Besides, the size effect of particle crushing strength can also be observed from the random field realizations with different values of SOF.

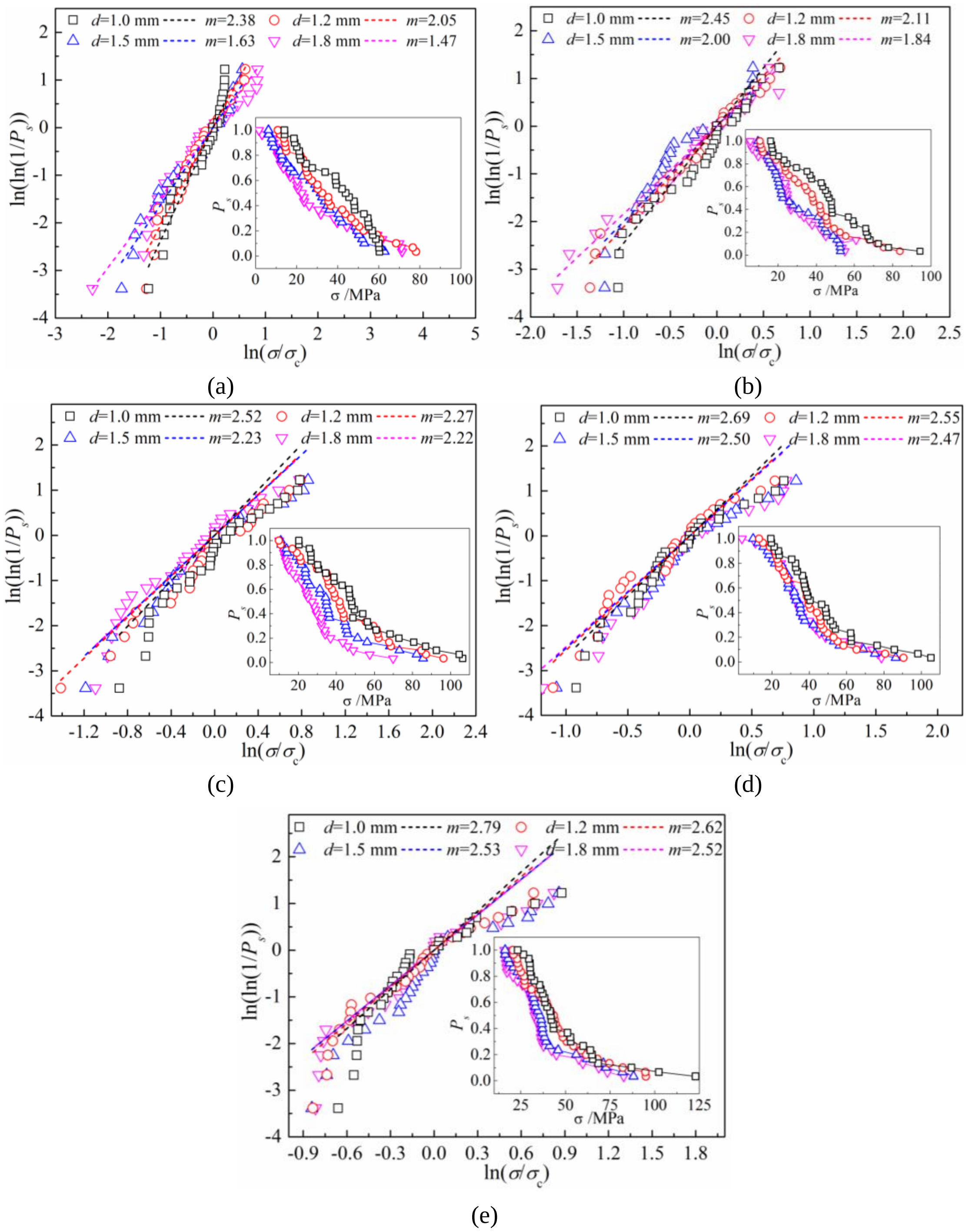

Fig. 11 Crushing strength distribution for numerical particles with random microscopic properties modelled by the RFT with different values of *SOF*: (a) *SOF*=0.00005 m; (b) *SOF*=0.0001 m; (c) *SOF*=0.0003 m; (d) *SOF*=0.0005 m; (e) *SOF*=0.001 m

Fig. 12 illustrates the dependency of Weibull parameters on the value of SOF. From Fig. 12(a), the characteristic crushing strength increases as the value of SOF increases. This also confirms the findings of Li et al., who stated that the compression strength of rock may increase with the increasing value of SOF [62]. Nie et al. [59] also demonstrated that the increasing value of SOF can be contributed to an improvement in the deformation and strength characteristics of sandy soil. As indicated by the previous investigations on the effect of SOF values on random field realizations, a larger value of SOF can result in a larger mean value of the associated microscopic properties in the random field realizations [78]. In this analysis, the increased characteristic crushing strength might be attributed to the higher magnitude of microscopic parameters in parallel bonds resulting from a larger value of SOF. In addition, an increase in the value of SOF also leads to a reduction in the spatial variability of random field realizations, which can also be observed from the Fig. 3(b). Therefore, it can be inferred that a larger value of SOF in the random field realizations corresponds to a larger Weibull modulus, suggesting a decreased variability in crushing strength of numerical particles, as shown in Fig. 12(b). Additionally, beyond a threshold value of 0.0005 m, the effects of SOF values on both the characteristics crushing strength and the Weibull modulus become negligible. Some researchers have also identified similar threshold SOF values through numerical simulations [62, 68, 79]. In the RFT-DEM model, the value of SOF quantifies the correction in local microscopic properties between any two points in the samples. As the value of SOF approaches the sample size, the sample would exhibit a near-homogeneous behavior, resulting in the crushing behavior not varying significantly with the value of SOF when it exceeds the threshold value.

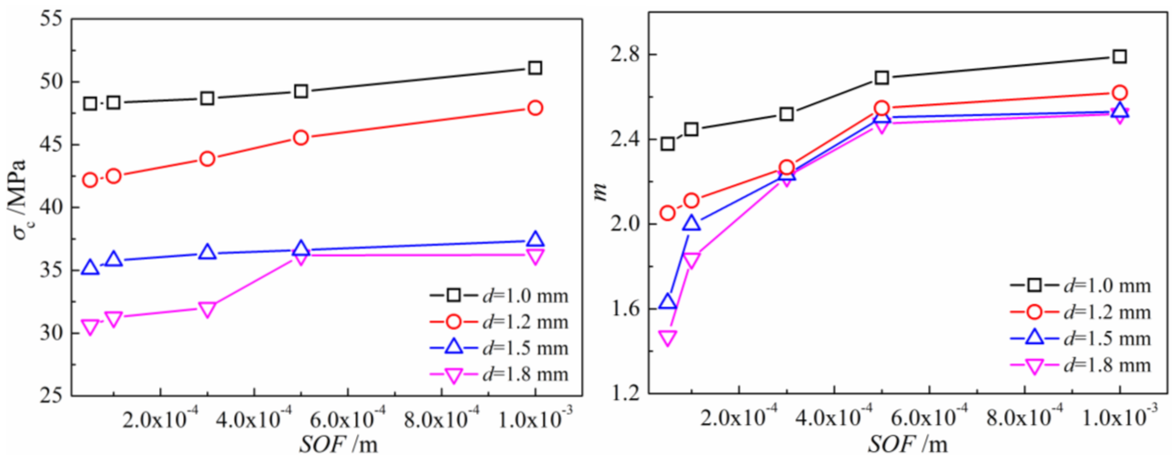

(a) (b)

Fig. 12 Weibull parameters versus SOF values: (a) Characteristic crushing strength;(b) Weibull modulus

For the numerical particles with randomly generated microscopic properties using different values of *SOF*, the characteristic crushing strength shows a negative linear relationship with the particle sizes in a double-logarithmic scale, as illustrated in Fig. 13. The slope value for the fitting lines increases with the increasing value of SOF, indicating that the size effect becomes less obvious as the value of SOF increases. As aforementioned, a larger value of SOF indicates a stronger spatial correlation of the microscopic properties, and hence the numerical sample becomes more homogenous. In accordance with the numerical particle preparation procedure in this study, the numerical particles of varying sizes are derived from a shared mother cubic sample. Hence, the difference in the statistics of microscopic properties between numerical particles with different sizes is smaller pronounced for a more homogenous mother cubic sample.

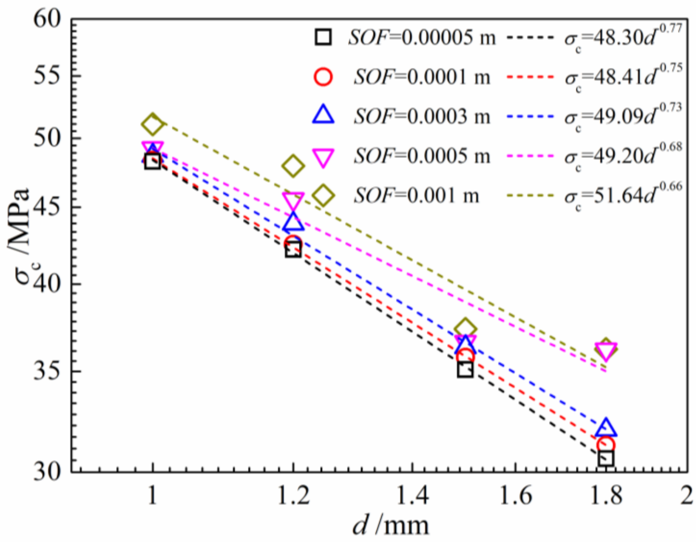

Fig. 13 The influence of SOF values on the size effect

Conclusions

In conclusion, this study introduced an innovative RFT-DEM model to simulate the variability in single particle crushing behavior, yielding valuable insights into the characteristics of granular materials under compression. The following practical conclusions can be drawn from our findings:

(1) The successful integration of random field theory into the discrete element method proved effective in capturing the spatial heterogeneity of individual sand particles. Utilizing random field parameters to represent microscopic strength properties in parallel bonds, the proposed RFT-DEM model was validated against experimental data, convincingly reproducing both inherent variability and size-dependent effects in single particle crushing behavior.

(2) The statistical analysis of material coefficients across different particle sizes revealed that larger particles exhibit more heterogeneous microscopic properties. Consequently, these particles display a greater variability in crushing strength. The presence of weak zones within larger particles contributed to a higher probability of crack initiation and propagation, ultimately leading to reduced particle crushing strength. This phenomenon

underscores the pivotal role of cumulative weak regions in determining the size effect on particle strength.

(3) A comprehensive parametric study involving COV ranging from 0.001 to 1.0 and SOF ranging from 0.00005 m to 0.001 m unveiled significant insights. It was observed that characteristic crushing strength and the Weibull modulus tend to decrease with increasing COV. Larger particles were more sensitive to COV variations than smaller counterparts, resulting in a pronounced size effect at higher COV values. However, the influence of COV became negligible when it was below or equal to 0.03. Meanwhile, with respect to SOF, both characteristics showed an increase as SOF values rose. Beyond a threshold SOF value of 0.0005 m, the effect of SOF on crushing strength and the Weibull modulus became marginal. Furthermore, an interesting trend emerged, indicating that the size effect diminished as SOF values increased.

The integration of Random Field Theory (RFT) and Discrete Element Method (DEM) in the proposed RFT-DEM model provides a robust framework for simulating and scrutinizing the intricate behavior of granular materials during single-particle crushing. These insights contribute significantly to understanding particle strength variability, size dependency, and the influence of material parameters, offering valuable perspectives for designing and analyzing granular systems in diverse engineering applications. However, the precise determination of actual Coefficient of Variation (COV) and Scale of Fluctuation (SOF) values for microscopic properties within particles remains a crucial challenge when employing a random field to characterize spatial heterogeneity. The selection of an appropriate autocorrelation function also poses a complex task. Furthermore, there is a need for further investigation into incorporating factors such as saturated conditions and particle morphology into the proposed RFT-DEM model. These considerations underscore the importance of ongoing research to refine the model's accuracy and extend its applicability to real-world scenarios.

Acknowledgments

This work was primarily supported by the National Natural Science Foundation of China (No. 51971188 and 51071134), the Scientific Research Foundation for Young Scholars of Xiangtan University (No. 21QDZ44), the Natural Science Foundation of Hunan Province, China (No. 2022JJ40440), the UK Engineering and Physical Sciences Research Council (EPSRC) New Investigator Award (Grant No. EP/V028723/1), the Foundation of

Hunan Educational Committee (No. 22B0151) and the Degree and Postgraduate Education Reform Project of Hunan Province (Grant No. CX20210648 and XDCX2019B105).

Conflicts of interest

The authors declare no conflict of interest.

Data Availability Statement

All data generated or analyzed during this study are included in this article.

References

[1] Cao D F, Shukla S K, Yang L Q, et al. Responses of calcareous sand foundations to variations of groundwater table and applied loads[J]. Journal of Rock Mechanics and Geotechnical Engineering, 2022, 14(4):1266-1279

[2] Emmanuel E, Anggraini V, Asadi A. An investigation on the breakage behavior of olivine sand particles: An attainable region technique[J]. Advanced Powder Technology, 2022, 33(2):103422.

[3] Zhang T, Zhang C, Luo T T. Effect of stress anisotropy on deformation and particle breakage of silica sand at high-pressure compression tests[J]. Construction and Building Materials, 2022, 316:125835.

[4] Barbosa L A P, Gerke K M, Munkholm L J, et al. Discrete element modeling of aggregate shape and internal structure effects on Weibull distribution of tensile strength[J]. Soil and Tillage Research, 2022, 219:105341.

[5] Guo W L, Zhu J G, Chen S S, et al. Applications of a gradation equation in coarse-grained soils[J]. Geotechnical Engineering, 2019, 172(5):1-37.

[6] Zhang S H, Zhao L H, Wang X, et al. Quantifying the effects of elongation and flatness on the shear behavior of realistic 3D rock aggregates based on DEM modeling[J]. Advanced Powder Technology, 2021, 32(5):1318-1332.

[7] Latvala J, Luomala H, Kolisoja P, et al. Convective heat transfer in crushed rock aggregates: The effects of grain size distribution and moisture content[J]. Journal of Cold Regions Engineering, 2020, 34(3):1-11.

[8] Zhao L H, Zhang S H, Huang D L, et al. 3D shape quantification and random packing simulation of rock aggregates using photogrammetry-based reconstruction and discrete element method[J]. Construction and Building Materials, 2020, 262:119986.

[9] Chen L, Zhao J C, Zhang H Y, et al. Experimental study on suffusion of gravelly soil[J]. Soil Mechanics and Foundation Engineering, 2015, 52(3):135-143.

[10] Xiao Y, Meng M Q, Daouadji A, et al. Effects of particle size on crushing and deformation behaviors of rockfill materials[J]. Geoscience Frontiers, 2020, 11(2):375-388.

[11] Frossard E, Hu W, Dano C, et al. Rockfill shear strength evaluation: A rational method based on size effects[J]. Geotechnique, 2012, 62(5):415-427.

[12] Oskooei P R, Mohammadinia A, Arulrajah A, et al. DEM modeling and experimental analysis of the breakage behavior of recycled crushed brick particles[J]. Transportation Geotechnics, 2021, 30:100586

[13] Bian X C, Li W, Qian Y, et al. Analysing the effect of principal stress rotation on railway track settlement by discrete element method[J]. Geotechnique, 2020, 70(9):803-821.

[14] Xu L J, Wang X Z, Wang R, et al. Physical and mechanical properties of calcareous soils: A review[J]. Marine Georesources and Geotechnology, 2021, 1(11):1-16.

[15] Wang B, Martin U, Rapp S. Discrete element modeling of the single-particle crushing test for ballast stones[J]. Computers and Geotechnics, 2017, 88:61-73.

[16] Wang G, Wang Z N, Ye Q G, et al. Particle breakage evolution of coral sand using triaxial compression tests[J]. Journal of Rock Mechanics and Geotechnical Engineering, 2021, 13(2):321-334.

[17] Jafarian Y, Javdanian H. Dynamic Properties of calcareous sand from the Persian Gulf in comparison with siliceous sands Database[J]. International Journal of Civil Engineering, 2020, 18(2):245-249.
[18] Karimpour H, Lade P V. Creep behavior in Virginia Beach sand[J]. Canadian Geotechnical Journal, 2013, 50(11):1159-1178.
[19] Ye J H, Haiyilati Y, Cao M, et al. Creep characteristics of calcareous coral sand in the South China Sea[J]. Acta Geotechnica, 2022, 17(11):5133-5155.
[20] Zhao B, Wang J, Coop M R. An investigation of single sand particle fracture using x-ray micro-tomography[J]. Geotechnique, 2015, 65(8):625-641.
[21] Thakur M M, Penumadu D. Triaxial compression in sands using FDEM and micro-X-ray computed tomography[J]. Computers and Geotechnics, 2020, 124:103638.
[22] Cheng Z, Wang J F. An investigation of the breakage behaviour of a pre-crushed carbonate sand under shear using X-ray micro-tomography[J]. Engineering Geology, 2021, 293:106286.
[23] Wang W A, Coop M R. An investigation of breakage behaviour of single sand particles using a high-speed microscope camera[J]. Geotechnique, 2016, 66(12):984-998.
[24] Shi F, Liu J S. A fully coupled hydromechanical XFEM model for the simulation of 3D non-planar fluid-driven fracture propagation[J]. Computers and Geotechnics, 2021, 132:103971.
[25] Zhang Y M, Lackner R, Zeiml M, et al. Strong discontinuity embedded approach with standard SOS formulation: Element formulation, energy-based crack-tracking strategy, and validations[J]. Computer Methods in Applied Mechanics and Engineering, 2015, 287:335-366.
[26] Xu F X, Hajibeygi H, Sluys L J. Multiscale extended finite element method for deformable fractured porous media[J]. Journal of Computational Physics, 2021, 436:110287.
[27] Li F, Pan J, Sinka C. Modelling brittle impact failure of disc particles using material point method[J]. International Journal of Impact Engineering, 2011;38:653-660.
[28] Li S, Zhang Y, Wu J C, et al. Modeling of crack propagation with the quasi-static material point method[J]. Engineering Fracture Mechanics, 2021, 245:107602.
[29] Guo Y J, Nairn J A. Three-Dimensional Dynamic Fracture Analysis Using the Material Point Method[J]. Computer Modeling in Engineering and Sciences, 2006, 16(3):141-155.
[30] Wang Y T, Zhou X P, Zhang T. Size effect of thermal shock crack patterns in ceramics: Insights from a nonlocal numerical approach[J]. Mechanics of Materials, 2019, 137:103133.
[31] Rabczuk T, Ren H L. A peridynamics formulation for quasi-static fracture and contact in rock[J]. Engineering Geology, 2017, 225:42-48.
[32] Ren H L, Zhang X Y, Cai Y C, et al. Dual-horizon peridynamics[J]. International Journal for Numerical Methods in Engineering, 2016, 108(12):1451-1476.
[33] Zhang T, Huang W X. DEM analysis of single-particle crushing considering the inhomogeneity of material properties[J]. Acta Mechanica Solida Sinica, 2022, 35(1):26-39.
[34] Gong Z D, Yang Y, Cui L J. et al. DEM investigation on the size effect in the fragmentation of intact aggregates[J]. Powder Technology, 2023, 425:118585.
[35] Liu G Y, Xu W J, Govender N, et al. A cohesive fracture model for discrete element method based on polyhedral blocks[J]. Powder Technology, 2020, 359:190-204.
[36] De T, Chakraborty J, Kumar J, et al. A particle location based multi-level coarse-graining technique for Discrete Element Method (DEM) simulation[J]. Powder Technology, 2022, 398:117058.
[37] Wu Q J, Chen Y M, Wilson J P. An effective parallelization algorithm for DEM generalization based on CUDA[J]. Environmental Modelling and Software, 2019, 114:64-74.
[38] Peters B, Kabore B W, Michael M, et al. A discrete element framework for modeling the mechanical behaviour of snow Part II: model validation[J]. Granular Matter, 2021, 23(2):1-15.
[39] Manso J, Marcelino J, Caldeira L. Effect of the clump size for bonded particle model on the uniaxial and tensile strength ratio of rock[J]. International Journal of Rock Mechanics and Mining Sciences, 2019, 114:131-140.
[40] Cil M B, Sohn C, Buscarnera G. DEM modeling of Grain size effect in brittle granular Soils[J]. Journal of Engineering Mechanics, 2020, 146(3): 04019138.
[41] Tavares L M, das Chagas A S. A stochastic particle replacement strategy for simulating breakage in DEM[J]. Powder

Technology, 2021, 377:222-232.
[42] Hanley K J, O'Sullivan C, Huang X. Particle-scale mechanics of sand crushing in compression and shearing using DEM[J]. Soils and Foundations, 2015, 55(5):1100-1112.
[43] Lin J, Bauer E, Wu W. A combined method to model grain crushing with DEM[J]. Geoscience Frontiers, 2020, 11(2):451-459.
[44] Kuang D M, Long Z L, Ogwu I, et al. A discrete element method (DEM)-based approach to simulating particle breakage[J]. Acta Geotechnica, 2022, 17(7):2751-2764.
[45] Aela P, Wang J H, Yousefian K, et al. Prediction of crushed numbers and sizes of ballast particles after breakage using machine learning techniques[J]. Construction and Building Materials, 2022, 337:127469.
[46] Wang P, Karatza Z, Arson C. DEM modelling of sequential fragmentation of zeolite granules under oedometric compression based on XCT observations[J]. Powder Technology, 2019, 347:66-75.
[47] Jiménez-Herrera N, Barrios G K.P, Tavares L M. Comparison of breakage models in DEM in simulating impact on particle beds[J]. Advanced Powder Technology, 2018, 29(3):692-706.
[48] Tong C X, Zhang K F, Zhang S, et al. A stochastic particle breakage model for granular soils subjected to one-dimensional compression with emphasis on the evolution of coordination number[J]. Computers and Geotechnics, 2019, 112:72-80.
[49] Lobo-Guerrero S, Vallejo L E. Application of Weibull Statistics to the Tensile Strength of Rock Aggregates[J]. Journal of Geotechnical and Geoenvironmental Engineering, 2006, 132(6):786-790.
[50] Lim W L, McDowell G R. The importance of coordination number in using agglomerates to simulate crushable particles in the discrete element method[J]. Geotechnique, 2007, 57(8):701-705.
[51] Mcdowell G R, Amon A. The application of Weibull statistics to the fractur of soil particles [J]. Soils and Foundations, 2000, 40(5):133-141.
[52] Qian J G, Gu J B, Gu X Q, et al. Discrete numerical modeling of granular materials considering crushability[J]. Journal of Mountain Science, 2017, 14(4): 758-770.
[53] Cheng Y P, Nakata Y, Bolton M D. Discrete element simulation of crushable soil[J]. Géotechnique, 2003, 53(7):633-641.
[54] Zhou M J, Song E X. A random virtual crack DEM model for creep behavior of rockfill based on the subcritical crack propagation theory[J]. Acta Geotechnica, 2016, 11(4):827-847.
[55] Zhou M J, Wen Y F, Deng G, et al. Three-dimensional discrete element simulation of random breaking strength and size effect in single particle splitting test of rockfill[J]. Rock and Soil Mechanics, 2019, 40(S1):503-510.
[56] Huang Q S, Zhou W, Ma G, et al. Experimental and numerical investigation of Weibullian behavior of grain crushing strength[J]. Geoscience Frontiers, 2020, 11(2):401-411.
[57] Laufer I. Grain crushing and high-pressure oedometer tests simulated with the discrete element method[J]. Granular Matter, 2015, 17(3):389-412.
[58] Onyejekwe S, Kang X, Ge L. Evaluation of the scale of fluctuation of geotechnical parameters by autocorrelation function and semivariogram function[J]. Engineering Geology, 2016, 214:43-49.
[59] Nie J Y, Cui Y F, Yang Z Y. Effect of heterogeneity of particle properties on variability of laboratory sandy soil properties: A random discrete element perspective[J]. Computers and Geotechnics, 2022, 141:104497.
[60] Zhao T, Crosta G B, Liu Y. Analysis of slope fracturing under transient earthquake loading by random discrete element method[J]. International Journal of Rock Mechanics and Mining Sciences, 2022, 157:105171.
[61] Zhao T, Liu Y. A novel random discrete element analysis of rock fragmentation[J]. International Journal for Numerical and Analytical Methods in Geomechanics, 2020, 44(10):1386-1395.
[62] Li L L, Guan J F, Liu Z Y. A random discrete element method for modeling rock heterogeneity[J]. Geomechanics and Geophysics for Geo-Energy and Geo-Resources, 2022, 8(1):1-13.
[63] Nakata Y, Hyde A F L, Hyodo M, et al. A probabilistic approach to sand particle crushing in the triaxial test[J]. Geotechnique, 1999, 49(5):567-583.
[64] Lv Y R, L X, Fan C F, et al. Effects of internal pores on the mechanical properties of marine calcareous sand particles[J]. Acta Geotechnica, 2021, 16(10):3209-3228.
[65] Fu R, Hu X L, Zhou B. Discrete element modeling of crushable sands considering realistic particle shape effect[J]. Computers and Geotechnics, 2017, 91:179-191.
[66] Balakrishnan A, Pizette P, Martin C L, et al. Effect of particle size in aggregated and agglomerated ceramic powders[J]. Acta Materialia, 2010, 58(3):802-812.

[67] Wang Y, Guan Z, Zhao T Y. Sample size determination in geotechnical site investigation considering spatial variation and correlation[J]. Canadian Geotechnical Journal, 2019, 56(7):992-1002.

[68] Huang H W, Xiao L, Zhang D M, et al. Influence of spatial variability of soil Young's modulus on tunnel convergence in soft soils[J]. Engineering Geology, 2017, 228:357-370.

[69] Wang F, Li H. A nonparametric approach for characterizing soil spatial variability based on cone penetration test data[J]. Bulletin of Engineering Geology and the Environment, 2021, 80(2):1073-1089.

[70] Jiang S H, Li D Q, Zhou C B, et al. Slope reliability analysis considering effect of autocorrelation functions[J]. Chinese Journal of Geotechnical Engineering, 2014, 36(3):508-518.

[71] Cavalcanti P P, Tavares L M. Statistical analysis of fracture characteristics of industrial iron ore pellets[J]. Powder Technology, 2018, 325:659-668.

[72] Ovalle C, Frossard E, Dano C, et al. The effect of size on the strength of coarse rock aggregates and large rockfill samples through experimental data[J]. Acta Mechanica, 2014, 225(8):2199-2216.

[73] Qian G, Lei W S, Yu Z S, et al. Statistical size scaling of breakage strength of irregularly-shaped particles[J]. Theoretical and Applied Fracture Mechanics, 2019, 102:51-58.

[74] Liu Y, Dai F, Xu N W, et al. Experimental and numerical investigation on the tensile fatigue properties of rocks using the cyclic flattened Brazilian disc method[J]. Soil Dynamics and Earthquake Engineering, 2018, 105:68-82.

[75] Lim W L, McDowell G R, Collop A C. The application of Weibull statistics to the strength of railway ballast[J]. Granular Matter, 2004, 6(4):229-237.

[76] Ergenzinger C, Seifried R, Eberhard P. A discrete element model predicting the strength of ballast stones[J]. Computers and Structures, 2012, 108-109:3-13.

[77] Syroka-Korol E, Tejchman J, Mróz, Z. FE investigations of the effect of fluctuating local tensile strength on coupled energetic-statistical size effect in concrete beams[J]. Engineering Structures, 2015, 103:239-259.

[78] Ching J Y, Phoon K K. Effect of element sizes in random field finite element simulations of soil shear strength[J]. Computers and Structures, 2013, 126(1):120-134.

[79] Liu Y, Lee F H, Quek S T, et al. Effect of spatial variation of strength and modulus on the lateral compression response of cement-admixed clay slab[J]. Geotechnique, 2015, 65(10):851-865.

[80] Vanmarcke E H. Probabilistic Modeling of Soil Profiles[J]. Journal of the Geotechnical Engineering Division Asce, 1977, 103(11):1227-1246.

[81] Fenton G A, Vanmarcke E H. Simulation of Random Fields via Local Average Subdivision[J]. Journal of Engineering Mechanics, 1990, 116(8):1733-1749.

[82] Yao W, Wang E, Liu X, Zhou R. Fracture distribution in overburden strata induced by underground mining[J]. Deep Underground Science and Engineering, 2022; 1: 58-64. doi:10.1002/dug2.12021